Interfacial wave theory of solidification: Dendritic pattern formation and selection of growth velocity

Jian-Jun Xu
Department of Mathematics and Statistics, McGill University, Montreal, Quebec, Canada H3A 2K6
(Received 3 November 1989; revised manuscript received 23 August 1990)

This work deals with the global instability mechanism of solidification from melt. It leads to a wave theory for solving long-standing problems—the pattern formation of dendritic growth and the selection of the tip velocity. One of the most important results drawn from the present work is that the selection condition of the dendrite's tip velocity can be found even in the absence of the anisotropy of surface tension. Two distinct sets of unstable global modes for the system are obtained: (1) the global trapped wave (GTW) modes, which describe the characteristics of waves trapped in the region between the tip point and the turning point; (2) modes that display a mechanism involving wave emission at the turning point and signal reflections between the turning point and the leading edge of the tip, abbreviated as WEASR. Uniformly valid asymptotic expansions for the GTW modes and the quantum conditions of corresponding eigenvalues are derived. The requirement that the total perturbed interfacial energy must be finite eventually rules out all the WEASR modes. The presence of the self-sustaining GTW mode in the system, however, very well explains the origin and persistence of the pattern formation in dendrite growth. A unique global neutral stable state is found, which gives the tip velocity at the later stage of growth. The present theory shows good agreement with the available experimental data for a nearly isotropic material.

I. INTRODUCTION

Dendritic growth is a common phenomenon in phase transition and crystal growth. Experimental observations show that at the later stage of growth, a dendrite has a smooth tip moving with a constant velocity. It emits a stationary wave train, propagating along the interface towards the root. The essence and origin of this nonlinear interfacial phenomenon have been a fundamental subject in the field of condensed-matter physics and material science for a long period of time.[1–20] The understanding of this problem has great significance for a much broader area, e.g., fluid dynamics, chemical engineering, biological science, etc., where similar pattern-formation phenomena occur.

In the past several decades, most researchers thought that the dendrite-tip region was steady and monotonic, so that it could be approximately described by a steady state of the system, whereas the dendrite-stem region was unsteady and oscillatory, and formed a so-called side-branching structure. Therefore, in studying the phenomenon of dendrite growth, the researchers normally treated the problem as two separate topics: (1) steady dendritic growth; it was anticipated that the steady-state solution could yield the characteristics of dendritic growth in the tip region, and (2) the formation of a side branching structure. The first problem was solved early in 1947 by Ivantsov for the zero-surface tension case.[1,2] The Ivantsov solution, however, does not provide sufficient information on the dendrite-tip region, as it cannot fully determine the tip velocity. As a consequence, the Ivantsov solution raised a new question as to what is the mechanism which determines the tip velocity. This selection problem of the tip velocity was understood as the selection problem of the steady state of the system for many years; a theory which predicts the tip speed of the steady state is the microscopic solvability condition (MSC) theory of Langer *et al.*[8] In order to determine the tip speed, however, it is necessary for the MSC theory that the system has a small amount of anisotropy of surface tension. Without the anisotropy of surface tension, according to the MSC theory, the system has no dendritic growth type of solutions. The theory presented here is an alternative to that theory and proceeds from a quite different physical description.

To study the global stability mechanisms of the system, one can, starting from linear instability theory, investigate the evolution of infinitesimal perturbations around the Ivantsov solution. In fluid dynamics, there are two approaches that have been used in the study of the evolution of perturbations. The first approach is to solve an initial-value problem: assume an given initial disturbance is introduced into the system, then consider the evolution of the initial disturbance by solving the initial value problem. The second approach is normal-mode analysis: assume the perturbations are in the form of quasistationary waves, and then investigate the evolution of such perturbations by solving a eigenvalue problem under a certain set of boundary conditions. The approach utilized in this work is very similar to that Lin used in developing his density wave theory for the spiral structure of galaxies in 1970s (see Ref. 21); it is also similar to what is used for establishing the critical-layer instability theory in fluid dynamics.[22] A major aim herein is to derive global-mode solutions. The eigenvalue corresponding to a global mode gives both the growth rate of the amplitude of perturbation and the frequency of the oscillation. It was first found by Xu (see Ref. 23) that in the dendritic system there exists a special simple turning point in the complex plane; in order to obtain the global-mode solutions of dendritic growth, one must apply the radiation condition

in the far field and the smooth condition at the tip of dendrite. This special turning point was missed in the analysis by Bensimon *et al.*[15] The discovery of this turning point is very crucial for the understanding of the dynamics of dendritic growth. Due to the existence of this turning point, in order to find global-mode solutions, one must divide the whole complex plane into three regions: the outer region, the turning point region, and the tip inner region. By using the multiple variable expansion (MVE) method, the outer solution in the outer region is found first. The local instability mechanism of the system is derived. The zeroth-order approximation results in a local dispersion relation for the normal-mode solutions, while the first-order approximation yields the amplitude functions of the solutions. It is the solution of the first-order approximation that gives a proof of the existence of a special simple turning point in the system. Near the turning point and the leading edge of the dendrite tip, the MVE fails; the solution has different asymptotic expansions. In the vicinity of the turning point, the system is reduced to the Airy equation with complex coefficients. Uniformly valid solutions in the neighborhood of the turning point are found. In the tip region, the tip inner solution is obtained; this tip solution satisfies the tip smoothness condition as a boundary condition. From the physical point of view, the tip smoothness condition produces a signal feedback process. Finally, all solutions are matched in the intermediate region; the global-mode solutions and a quantum condition for the eigenvalues are obtained. Two remarkable global instability mechanisms [the global trapped-wave (GTW) mechanism and the wave emission and signal reflection (WEASR) mechanism] for the system are then exploited, which results in two discrete sets of global modes: GTW modes and WEASR modes, respectively (see Refs. 24 and 25). A detailed investigation of the behavior of the modes in the far field eventually ruled out all the WEASR modes; it is concluded that only the GTW modes are physically meaningful. The presence of the self-sustaining GTW mode explains the origin and persistence of the pattern formation in the solidification process. At the same time, the global neutral stability (GNS) condition for the GTW mode yields a solution to the selection problem of the tip velocity.

The results obtained in this paper show that the selection of the tip velocity and the formation of the dendritic pattern are problems that cannot be separated; the actually selected solution for a realistic dendrite growth is not the stable, steady state of the system near the similarity solution as many investigators thought, but the time-dependent, global-neutrally-stable state of the system; the selection condition for the tip speed can be found even in the absence of anisotropy of surface tension.

The basic results of this work have been published in part in its first version.[23–27] In the present paper, we intend to give a more systematic description. Some typos and errors in mathematical details were found in Ref. 23, which are corrected in the present paper. This paper is arranged as follows. Section II presents the mathematical formulation; Sec. III gives the basic state and the linear perturbed system. The problem of dendritic growth is formulated as a linear eigenvalue problem; Sec. IV shows the normal-mode solution in the outer region; Sec. V gives the uniformly valid solution near the turning point; Sec. VI gives the tip solution; Sec. VII shows the global trapped wave modes and the quantum conditions for the eigenvalues; Sec. VIII shows another type of global modes—WEASR modes; Sec. IX demonstrates the essence and origin of the pattern formation in solidification, and gives the selection condition for the tip velocity; finally, in Sec. X, we summarize the results.

II. MATHEMATICAL FORMULATION OF THE PROBLEM

Consider a single dendrite growing in an undercooled pure melt in the negative z direction with a constant average velocity U (see Fig. 1). For simplicity, we assume the mass density ρ, the thermal diffusivity κ_T, the specific heat c_p, and other thermal characteristic constants of the solid state are the same as that of the liquid state, gravity is negligible and the surface tension is isotropic. We utilize the thermal length $l_T=\kappa_T/U$ as the length scale, $\Delta H/c_p$ as the scale of the temperature, where ΔH is the latent heat per unit volume of the solid, and adopt the paraboloidal coordinate system (ξ,η) defined, through the cylindrical coordinate system $(\mathbf{r},z)$, as follows (see Fig. 2):

$$r/\eta_0^2=\xi\eta;\quad z/\eta_0^2=\tfrac{1}{2}(\xi^2-\eta^2)\ . \tag{2.1}$$

$T(\xi,\eta,t)$, $T_S(\xi,\eta,t)$ are used to represent the temperature fields in the melt and solid state, respectively, while $\eta_s(\xi,t)$ represents the interface shape. Thus, a general unsteady state is described by the following equation:

$$\left[\frac{\partial^2 T}{\partial\xi^2}+\frac{\partial^2 T}{\partial\eta^2}+\frac{1}{\xi}\frac{\partial T}{\partial\xi}+\frac{1}{\eta}\frac{\partial T}{\partial\eta}\right]$$

$$=\eta_0^2\left[\xi\frac{\partial T}{\partial\xi}-\eta\frac{\partial T}{\partial\eta}\right]+\eta_0^4(\xi^2+\eta^2)\frac{\partial T}{\partial t}\ . \tag{2.2}$$

The boundary conditions and regularity conditions are

$$(1)\ \text{As}\ \eta\to\infty,\quad T\to T_\infty\ . \tag{2.3}$$

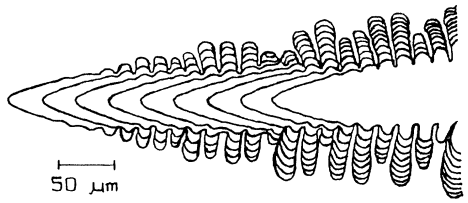

FIG. 1. A typical growing dendrite.

(2) As $\eta\to 0$, $\dfrac{\partial T_s}{\partial \eta}\to 0$; $T_S=O(1)$. (2.4)

(3) On the interface $\eta=\eta_s(\xi,t)$,

(i) the thermodynamic equilibrium condition applies:

$$T=T_S \ , \tag{2.5}$$

(ii) the Gibbs-Thompson condition applies:

$$T=-\frac{\Gamma}{\eta_0^2}K\left\{\frac{d}{d\xi},\frac{d^2}{d\xi^2}\right\}\eta_s \ , \tag{2.6}$$

where the curvature operator

$$K\left\{\frac{d}{d\xi},\frac{d^2}{d\xi^2}\right\}\eta_s=\frac{1}{(\xi^2+\eta_s^2)^{1/2}}\left[\frac{\eta_s''}{(1+\eta_s'^2)^{3/2}}-\frac{1}{\eta_s(1+\eta_s'^2)^{1/2}}+\frac{\eta_s'(\eta_s^2+2\xi^2)-\xi\eta_s}{\xi(\xi^2+\eta_s^2)(1+\eta_s'^2)^{1/2}}\right] , \tag{2.7}$$

(iii) and the heat balance condition applies:

$$\frac{\partial}{\partial\eta}(T-T_S)-\eta_s'\frac{\partial}{\partial\xi}(T-T_S)+\eta_0^2(\xi\eta_s)'+\eta_0^4(\xi^2+\eta^2)\frac{\partial\eta_s}{\partial t}=0 \ . \tag{2.8}$$

In the above, the prime represents the derivative with respect to ξ; the surface-tension parameter Γ is defined as

$$\Gamma=l_c/l_T; \quad l_c=\frac{\gamma c_p T_{M0}}{(\Delta H)^2} \ , \tag{2.9}$$

where γ is the surface tension, T_{M0} is the melting temperature of flat interface, and l_c is the capillary length. A special type of time-dependent problem will be considered, as is described later.

III. BASIC STATE AND LINEAR PERTURBED SYSTEM

For the case of zero surface tension ($\Gamma=0$), the well-known steady similarity solution exists for arbitrary undercooling. The shape of its interface is a paraboloid. This solution will be used as the basic state for our problem. Without losing generality, one can adjust the parameter η_0 in (2.1) such that the basic state of the system is expressed as follows:

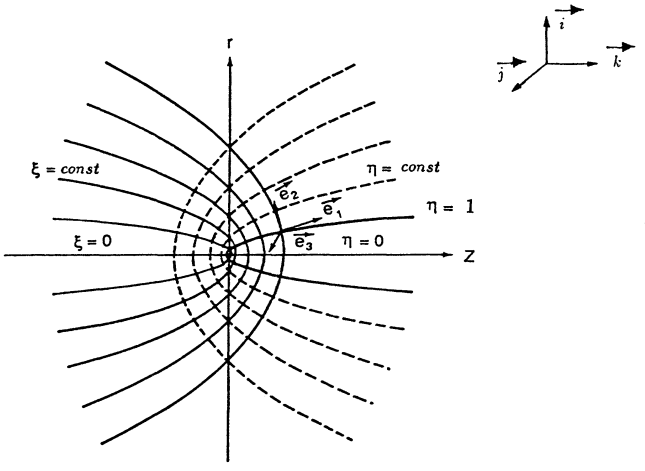

FIG. 2. The paraboloidal coordinate system used in the present paper.

$$T_B=T_B(\eta)=T_\infty+\frac{\eta_0^2}{2}e^{\eta_0^2/2}E_1\left[\frac{\eta_0^2\eta^2}{2}\right] ,$$
$$T_{SB}=T_B(1) \ ,$$
$$\eta_B=1 \ , \tag{3.1}$$
$$T_\infty+\frac{\eta_0^2}{2}e^{\eta_0^2/2}E_1\left[\frac{\eta_0^2}{2}\right]=0 \ ,$$

where the subscripts B and S refer to the basic state and the solid phase, respectively; $E_1(x)$ is the exponential integral (see Ref. 27). The constant η_0 in (2.1) then can be expressed as a function of the undercooling T_∞. The radius of curvature of the paraboloid l_b at the tip $\xi=0$ is found to be

$$l_b=\eta_0^2 l_T \ . \tag{3.2}$$

But dendrite growth with nonzero surface tension is intrinsically an unsteady process. In the present paper, we assume that at the later stage of growth, this unsteady process can be described by a time-periodic solution near the above Ivantsov similarity solution. Therefore, we separate the general unsteady state into two parts: the basic state (3.1) and the perturbation $\{\tilde{h}_s,\tilde{T},\tilde{T}_S\}$,

$$T(\xi,\eta,t)=T_B+\tilde{T}(\xi,\eta,t) \ ,$$
$$T_S(\xi,\eta,t)=T_{SB}+\tilde{T}_S(\xi,\eta,t) \ , \tag{3.3}$$
$$\eta_s=\eta_B+\tilde{h}(\xi,t)/\eta_0^2 \ .$$

Due to the smallness of the parameter Γ, the perturbation part in (3.3) has small amplitude in any finite region around the tip, compared with the basic state. Thus, define a surface-tension stability parameter

$$\epsilon=\frac{\sqrt{\Gamma}}{\eta_0^2} \ . \tag{3.4}$$

To study the behavior of the perturbation part, one can introduce a set of fast variables $\{\xi_+,\eta_+,t_+\}$:

$$\xi_+=\frac{\xi}{\epsilon}, \quad \eta_+=\frac{\eta-1}{\epsilon}, \quad t_+=\frac{t}{\epsilon} \ , \tag{3.5}$$

and use multiple-variable asymptotic expansion for the solution near the similarity solution. It is easily shown

that the basic system for the perturbation is inhomogeneous and the perturbation part can be expressed in the asymptotic form:

$$\tilde{q}=\epsilon^2[\hat{q}_0(\xi,\eta)+\epsilon^2\hat{q}_1(\xi,\eta)+\cdots] +[\tilde{q}_0(\xi,\eta,\xi_+,\eta_+,t)+\epsilon\tilde{q}_1(\xi,\eta,\xi_+,\eta_+,t)+\cdots], \tag{3.6}$$

where the notation $\tilde{q}$ represents the all perturbation quantities in (3.3). This implies that the solution for the perturbation part in (3.3) contains two components:

(1) The steady perturbation component $\{\hat{q}_0,\hat{q}_1,\ldots\}$, which is a particular solution of the above-mentioned basic inhomogeneous system. This component is the steady regular perturbation expansion around the similarity solution in small surface tension ϵ^2. This component only contains the slow variables (ξ,η); it was solved in Ref. 13.

(2) The unsteady perturbation component $\{\tilde{q}_0,\tilde{q}_1,\ldots\}$, which contains the multiple variables and is defined by an associated homogeneous system. This component is the time-dependent singular perturbation expansion. One may only consider the unsteady perturbation component, as the unsteady perturbation component is decoupled from and dominates the steady perturbation component.

In terms of the fast variables, the perturbed system is expressed in the following form:

$$\left[\frac{\partial^2}{\partial\xi_+^2}+\frac{\partial^2}{\partial\eta_+^2}\right]\tilde{T}=\epsilon\left[\eta_0^4(\xi^2+\eta^2)\frac{\partial}{\partial t_+} +\eta_0^2\left[\xi\frac{\partial}{\partial\xi_+}-\eta\frac{\partial}{\partial\eta_+}\right] -\frac{1}{\xi}\frac{\partial}{\partial\xi_+}-\frac{1}{\eta}\frac{\partial}{\partial\eta_+}\right]\tilde{T}\ ; \tag{3.7}$$

the boundary conditions are

(1) As $\eta_+\to\infty$, $\tilde{T}\to 0$. (3.8)

(2) As $\eta_+\to-\infty$, $\tilde{T}_S\to 0$. (3.9)

(3) On the interface $\eta_+=0$, $\eta=1$,

(i) $$\tilde{T}=\tilde{T}_S+\tilde{h}+O(\epsilon)\ , \tag{3.10}$$

(ii) $$\tilde{T}_S=\frac{1}{S(\xi)}\left[\frac{\partial^2\tilde{h}}{\partial\xi_+^2}+\frac{\epsilon(1+2\xi^2)}{\xi S^2(\xi)}\frac{\partial\tilde{h}}{\partial\xi_+}-\frac{\epsilon^2}{S^2(\xi)}\tilde{h}\right] +O(\epsilon^3)\ , \tag{3.11}$$

(iii) $$\frac{\partial}{\partial\eta_+}(\tilde{T}-\tilde{T}_S)+\eta_0^2S^2(\xi)\frac{\partial\tilde{h}}{\partial t_+} +\xi\frac{\partial\tilde{h}}{\partial\xi_+}+\epsilon(2+\eta_0^2)\tilde{h}+O(\epsilon^2)=0\ , \tag{3.12}$$

where

$$S(\xi)=(\xi^2+1)^{1/2}\ . \tag{3.13}$$

It shall be shown below how to find the global-mode solutions for the system (3.7)–(3.12). These solutions must be uniformly valid in the whole physical region $(0\le\xi<\infty)$; moreover, these solutions must satisfy certain boundary conditions at the tip and in the far field. Based on experimental investigations (see Fig. 1) and physical considerations, the following conditions are imposed:

(4) the tip smoothness condition:

$$\text{as } \xi\to 0^+,\quad \tilde{h}(0)<\infty;\quad \tilde{h}'(0)=0\ , \tag{3.14}$$

and

(5) a radiation condition in the far field: as $\xi\to\infty$, the solution describes an outgoing wave. Namely,

$$\tilde{h}(\xi)\sim\exp\left[\frac{\sigma t}{\epsilon\eta_0^2}+\frac{i}{\epsilon}\int_0^{\xi}k_0(\xi_1)d\xi_1\right]\ , \tag{3.15}$$

where $\sigma=\sigma_R-i\omega$ is an eigenvalue with $\omega>0$, while $k_0(\xi)$ is a wave-number function to be determined by the local dispersion relation of the system [see (4.14)]. In addition, it is also required that the total perturbed surface energy must be finite, so that the amplitude of the outgoing wave must decay as $\xi\to\infty$. In the following sections, we will find the solution for this problem.

IV. OUTER EXPANSION SOLUTION

In order to derive the outer solution for the perturbed state in the outer region, we have to utilize a new set of fast variables $(\xi_{++},\eta_{++},t_{++})$, such that

$$d\xi_{++}=k(\xi,\epsilon)d\xi_+,\quad \eta_{++}=k(\xi,\epsilon)\eta_+\ ,\quad t_{++}=t_+/\eta_0^2\ , \tag{4.1}$$

and make the following asymptotic expansion:

$$\begin{aligned}\tilde{T}&=[\tilde{T}_0(\xi,\eta,\xi_{++},\eta_{++}) +\epsilon\tilde{T}_1(\xi,\eta,\xi_{++},\eta_{++})+\cdots]e^{\sigma t_{++}}\ ,\\ \tilde{h}&=[\tilde{h}_0(\xi,\xi_{++})+\epsilon\tilde{h}_1(\xi,\xi_{++})+\cdots]e^{\sigma t_{++}}\ ,\\ k&=k_0+\epsilon k_1+\epsilon^2k_2+\cdots\ .\end{aligned} \tag{4.2}$$

According to the multiple variable expansion (MVE) method (Ref. 28), the fast and slow variables $(\xi,\eta,\xi_{++},\eta_{++},t_{++})$ in the solutions are treated formally as independent variables. Hence, the derivatives in the system (3.7)–(3.12) must be replaced by

$$\begin{aligned}\frac{\partial}{\partial\xi_+}&=k\frac{\partial}{\partial\xi_{++}}+\epsilon\frac{\partial}{\partial\xi}\ ,\\ \frac{\partial}{\partial\eta_+}&=k\frac{\partial}{\partial\eta_{++}}+\epsilon\frac{\partial}{\partial\eta}\ ,\\ \frac{\partial^2}{\partial\xi_+^2}&=\left[k\frac{\partial}{\partial\xi_{++}}+\epsilon\frac{\partial}{\partial\xi}\right]^2\ ,\\ \frac{\partial^2}{\partial\eta_+^2}&=\left[k\frac{\partial}{\partial\eta_{++}}+\epsilon\frac{\partial}{\partial\eta}\right]^2\ .\end{aligned} \tag{4.3}$$

The system for the perturbation part with the multiple variables is listed in the Appendix. By substituting (4.2)

into the system (A1)–(A6), one can successively derive each order approximation in the outer region ($\xi \gg \epsilon$). The results are listed as below.

A. $O(\epsilon^0)$

As the zeroth-order approximation, one can derive the following system, which describes quasisteady heat conduction:

$$\left[\frac{\partial^2}{\partial\xi_{++}^2}+\frac{\partial^2}{\partial\eta_{++}^2}\right]\tilde{T}_0=0\ ,$$
$$\left[\frac{\partial^2}{\partial\xi_{++}^2}+\frac{\partial^2}{\partial\eta_{++}^2}\right]\tilde{T}_{S0}=0\ . \tag{4.4}$$

The boundary conditions are

(1) As $\eta_{++}\to\infty$, $\tilde{T}_0\to 0$; (4.5)

(2) As $\eta_{++}\to-\infty$, $\tilde{T}_{S0}\to 0$; (4.6)

(3) On the interface $\eta_{++}=0$, $\eta=1$,

(i) $\tilde{T}_0=\tilde{T}_{S0}+\tilde{h}_0$, (4.7)

(ii) $\tilde{T}_{S0}=\dfrac{k_0^2}{S(\xi)}\dfrac{\partial^2\tilde{h}_0}{\partial\xi_{++}^2}$, (4.8)

(iii) $k_0\dfrac{\partial}{\partial\eta_{++}}(\tilde{T}_0-\tilde{T}_{S0})$

$$+\sigma S^2(\xi)\tilde{h}_0+k_0\xi\frac{\partial\tilde{h}_0}{\partial\xi_{++}}=0\ . \tag{4.9}$$

This system has the following normal-mode solutions:

$$\tilde{T}_0=A_0(\xi,\eta)\exp\{i\xi_{++}-\eta_{++}\}\ ,$$
$$\tilde{T}_{S0}=B_0(\xi,\eta)\exp\{i\xi_{++}+\eta_{++}\}\ , \tag{4.10}$$
$$\tilde{h}_0=\hat{D}_0\exp\{i\xi_{++}\}\ .$$

The coefficient $\hat{D}_0$ in the zeroth-order approximation is set as a constant without loss of generality, because the complex wave function $k(\xi)$ contains the varying component of the amplitude of the solution $\tilde{h}_0$. By setting

$$\hat{A}_0(\xi)=A_0(\xi,1),\quad \hat{B}_0(\xi)=B_0(\xi,1)\ , \tag{4.11}$$

from (4.7)–(4.9), we derive that

$$\hat{A}_0(\xi)=\left[1-\frac{k_0^2}{S}\right]\hat{D}_0\ , \tag{4.12}$$

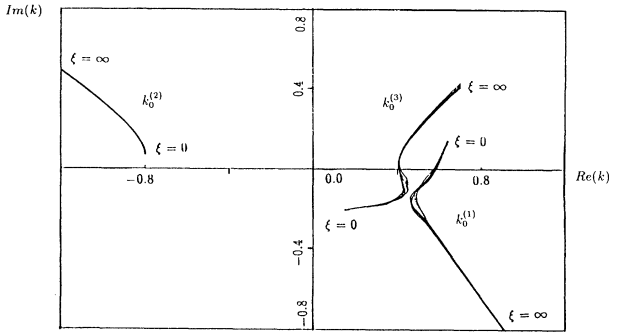

FIG. 3. The curves of wave-number functions $\{k_0^{(1)},k_0^{(2)},k_0^{(3)}\}$ for a set of the eigenvalues σ.

$$\hat{B}_0(\xi)=-\frac{k_0^2}{S}\hat{D}_0\ , \tag{4.13}$$

where $\hat{D}_0$ is an arbitrary constant; the wave-number function $k_0(\xi)$ is subject to the local dispersion formula

$$\sigma=\Sigma(\xi,k_0)=\frac{k_0}{S^2}\left[1-\frac{2k_0^2}{S}\right]-i\frac{\xi}{S^2}k_0\ . \tag{4.14}$$

The local dispersion formula (4.14) is a generalization of the Mullins-Sekerka dispersion relation for a plane interface. To show this, we use the arc length l along the Ivantsov paraboloid as an independent variable and rewrite the normal mode solution (4.10) in the form

$$\tilde{h}\approx\hat{D}_0\exp\left[\frac{1}{\epsilon\eta_0^2}\left[\sigma t+i\int k_*\,dl\right]\right]\ , \tag{4.15}$$

where

$$k_*=\frac{k_0}{S} \tag{4.16}$$

and $dl=\eta_0^2 S\,d\xi$. Accordingly, the local dispersion formula (4.14) is transformed into the form

$$\sigma=k_*(|V_n|-2k_*^2)-i|V_\tau|k_*\ . \tag{4.17}$$

Here

$$V_n=\frac{1}{S},\quad V_\tau=\frac{\xi}{S} \tag{4.18}$$

are the normal and tangent components of the local growth rate of the interface at ξ. For $V_\tau=0$, the formula (4.17) reduces to the Mullins-Sekerka dispersion relation.

For any given constant σ, one can find three roots from (4.14) (see Fig. 3), namely

$$k_0^{(1)}(\xi)=M(\xi)\cos\left[\tfrac{1}{3}\cos^{-1}\left[\frac{\sigma}{N(\xi)}\right]\right]\ \text{(short-wave branch)}\ ,$$
$$k_0^{(2)}(\xi)=M(\xi)\cos\left[\tfrac{1}{3}\cos^{-1}\left[\frac{\sigma}{N(\xi)}\right]+\frac{2\pi}{3}\right]\ , \tag{4.19}$$
$$k_0^{(3)}(\xi)=M(\xi)\cos\left[\tfrac{1}{3}\cos^{-1}\left[\frac{\sigma}{N(\xi)}\right]+\frac{4\pi}{3}\right]\ \text{(long-wave branch)}\ ,$$

where

$$M(\xi)=\left[\frac{2S(\xi)}{3}\right]^{1/2}(1-i\xi)^{1/2}\ ,\quad N(\xi)=-\frac{M(\xi)}{3S^2(\xi)}(1-i\xi)\ . \tag{4.20}$$

In order for the temperature $\tilde{T}_0$ to satisfy the boundary condition (4.5), one must have $\mathrm{Re}\{k_0\}>0$; consequently, only $k_0^{(1)}(\xi)$, $k_0^{(3)}(\xi)$ in (4.19) are meaningful. Thus, the general solution in the outer region is

$$\tilde{h}=D_0^{(1)}\exp\left[\sigma t_{++}+\frac{i}{\epsilon}\int_0^{\xi}(k_0^{(1)}+\epsilon k_1^{(1)}+\cdots)d\xi_1\right]+D_0^{(3)}\exp\left[\sigma t_{++}+\frac{i}{\epsilon}\int_0^{\xi}(k_0^{(3)}+\epsilon k_1^{(3)}+\cdots)d\xi_1\right]+\cdots\ . \tag{4.21}$$

B. $O(\epsilon)$

In the first-order approximation, one can determine the amplitude functions $A_0(\xi,\eta)$ and $B_0(\xi,\eta)$ and the function $k_1(\xi)$. The following equations are derived:

$$k_0^2\left[\frac{\partial^2}{\partial\xi_{++}^2}+\frac{\partial^2}{\partial\eta_{++}^2}\right]\tilde{T}_1=a_0e^{i\xi_{++}-\eta_{++}}\ ,\quad k_0^2\left[\frac{\partial^2}{\partial\xi_{++}^2}+\frac{\partial^2}{\partial\eta_{++}^2}\right]\tilde{T}_{S1}=b_0e^{i\xi_{++}+\eta_{++}}\ , \tag{4.22}$$

where

$$a_0=2k_0\left[\frac{\partial A_0}{\partial\eta}-i\frac{\partial A_0}{\partial\xi}\right]+A_0\left[\sigma\eta_0^2(\xi^2+\eta^2)+k_0\eta_0^2(i\xi+\eta_0^2)+\frac{k_0}{\eta}-\frac{ik_0}{\xi}-i\frac{\partial k_0}{\partial\xi}\right]\ , \tag{4.23}$$

$$b_0=-2k_0\left[\frac{\partial B_0}{\partial\eta}+i\frac{\partial B_0}{\partial\xi}\right]+B_0\left[\sigma\eta_0^2(\xi^2+\eta^2)+k_0\eta_0^2(i\xi-\eta_0^2)-\frac{k_0}{\eta}-\frac{ik_0}{\xi}-i\frac{\partial k_0}{\partial\xi}\right]\ . \tag{4.24}$$

To ensure the uniform validity of the expansions as $\xi\to\infty$, one must eliminate the secular term in the right-hand side of Eqs. (4.22), or say, set

$$a_0=b_0=0\ . \tag{4.25}$$

From the conditions (4.25), it follows that

$$\left[\frac{\partial}{\partial\eta}-i\frac{\partial}{\partial\xi}\right]\ln\Psi(\xi,\eta)=0\ , \tag{4.26}$$

$$\left[\frac{\partial}{\partial\eta}+i\frac{\partial}{\partial\xi}\right]\ln\Phi(\xi,\eta)=0\ , \tag{4.27}$$

where

$$\begin{aligned}&\Psi(\xi,\eta)=A_0(\xi,\eta)k_0^{1/2}\xi^{1/2}\eta^{1/2}F(\xi,\eta)\ ,\\&\Phi(\xi,\eta)=B_0(\xi,\eta)k_0^{1/2}\xi^{1/2}\eta^{1/2}G(\xi,\eta)\ ,\end{aligned} \tag{4.28}$$

$$F(\xi,\eta)=\exp\left[\frac{\eta_0^2}{4}(\eta^2-\xi^2)+\sigma\eta_0^2\left[\frac{\eta^3}{6k_0}+i\int_0^{\xi}\frac{\xi_1^2}{2k_0}d\xi_1\right]\right]\ , \tag{4.29}$$

$$G(\xi,\eta)=\exp\left[\frac{\eta_0^2}{4}(\eta^2-\xi^2)+\sigma\eta_0^2\left[-\frac{\eta^3}{6k_0}+i\int_0^{\xi}\frac{\xi_1^2}{2k_0}d\xi_1\right]\right]\ .$$

In terms of the boundary conditions (4.11), one can obtain the solutions

$$\Psi(\xi,\eta)=\hat{A}_0(\zeta_1)k_0^{1/2}(\zeta_1)\zeta_1^{1/2}F(\zeta_1,1)\ ,\quad \Phi(\xi,\eta)=\hat{B}_0(\zeta_2)k_0^{1/2}(\zeta_2)\zeta_2^{1/2}G(\zeta_2,1)\ , \tag{4.30}$$

with the notations

$$\zeta_1=\xi+i(\eta-1);\quad \zeta_2=\xi-i(\eta-1)\ . \tag{4.31}$$

Thus, the amplitude functions $A_0(\xi,\eta)$ and $B_0(\xi,\eta)$ are determined. from (4.23)–(4.25), it is also seen that

$$Q_0=\frac{\partial}{\partial\eta}(A_0-B_0)\bigg|_{\eta=1}=i\frac{\partial}{\partial\xi}(\hat{A}_0+\hat{B}_0)-(\hat{A}_0+\hat{B}_0)\left[\frac{\sigma\eta_0^2}{2k_0}S^2(\xi)+\frac{i}{2}\left[\xi\eta_0^2-\frac{1}{\xi}-\frac{d\log k_0}{d\xi}\right]\right]-\left[\frac{1+\eta_0^2}{2}\right](\hat{A}_0-\hat{B}_0)\ . \tag{4.32}$$

This formula is needed later to find $k_1(\xi)$. In terms of the conditions (4.25), one obtains the first-order approximate solution:

$$\tilde{T}_1 = A_1(\xi,\eta)\exp(i\xi_{++}-\eta_{++}) ,$$
$$\tilde{T}_{S1} = B_1(\xi,\eta)\exp(i\xi_{++}+\eta_{++}) , \tag{4.33}$$
$$\tilde{h}_1 = \hat{D}_1\exp(i\xi_{++}) .$$

Setting

$$\hat{A}_1(\xi) = A_1(\xi,1) , \quad \hat{B}_1(\xi) = B_1(\xi,1) , \tag{4.34}$$

from (A4)–(A6), one can derive the first-order approximate interface boundary conditions. Then, it is found that

$$\hat{B}_1 = -\frac{k_0^2}{S}\hat{D}_1 + I , \tag{4.35}$$

$$\hat{A}_1 = \hat{B}_1 + \hat{D}_1 , \tag{4.36}$$

$$I = \frac{\hat{D}_0}{S}\left[i\frac{dk_0}{d\xi} + ik_0\left[\frac{1}{\xi}+\frac{\xi}{S^2}\right] - 2k_0k_1 \right] , \tag{4.37}$$

and

$$k_1 = \frac{\left[\frac{3}{2}+\frac{\eta_0^2}{2}\right] + W_0(\xi) + \frac{i}{2\xi}\left[1-\frac{6k_0^2}{S}\right]}{\left[1-i\xi-\frac{6k_0^2}{S}\right]} , \tag{4.38}$$

where

$$W_0(\xi) = i\frac{d\ln k_0}{d\xi}\left[\frac{1}{2}-\frac{7k_0^2}{S}\right] - (1-2k_0^2)\left[\frac{\sigma\eta_0^2}{2k_0}S^2 + \frac{i}{2}\xi\eta_0^2\right] . \tag{4.39}$$

Notice that from the dispersion formula (4.14), it is derived that

$$S^2\left[\frac{\partial\Sigma}{\partial k_0}\right] = 1-i\xi-\frac{6k_0^2}{S} . \tag{4.40}$$

Thus, one can also write

$$k_1(\xi) = \frac{R_1(\xi)}{S^3\left[\frac{\partial\Sigma}{\partial k_0}\right]} + \frac{i}{2\xi} , \tag{4.41}$$

where the function $R_1(\xi)$ is regular in the complex ξ plane. From (4.41), it is seen that the system in hand has four singular points, where the outer solution (4.21) becomes invalid, namely:

(i) The tip of the dendrite, $\xi=0$. The appearance of this singular point is caused by our asymptotic treatment, which fails for $|\xi| \ll \epsilon$. As $\xi\to 0$, due to

$$k_1 \sim \frac{i}{2\xi} , \tag{4.42}$$

one has

$$\tilde{h} = \left[\frac{D_0^{(1)}}{\sqrt{\xi}}\exp\left[i\int_0^{\xi}k_0^{(1)}d\xi_+\right] + \frac{D_0^{(3)}}{\sqrt{\xi}}\exp\left[i\int_0^{\xi}k_0^{(3)}d\xi_+\right] + \cdots\right] e^{\sigma t_{++}} . \tag{4.43}$$

(ii) The critical points $\xi=\xi_c^{(i)}$, which are the roots of the equation:

$$\frac{\partial\Sigma(\xi,k_0)}{\partial k_0} = 0 . \tag{4.44}$$

Combining (4.14) and (4.44), one finds that $\xi_c^{(i)}$, $(i=1,2,3)$ are the three roots of the equation

$$\sigma = \left[\frac{2}{27}\right]^{1/2}\left[\frac{1-i\xi_c}{S}\right]^{3/2}_{\xi=\xi_c} = \left[\frac{2}{27}\right]^{1/2}\left[\frac{1-i\xi_c}{1+i\xi_c}\right]^{3/4} . \tag{4.45}$$

These critical points are related to the eigenvalue σ. It will be shown later that these critical points are simple turning points of the system in the complex ξ plane and one of these critical points, $\xi_c^{(1)}$ emanates a Stokes line L_1, which intersects with the positive part of the real ξ axis at the point ξ_c'. The presence of this turning point is essential to the characteristics of unsteady dendritic growth, which was missed in the analysis by Bensimon *et al.*[15] The existence and significance of this critical point ξ_c was identified by Xu; see Ref. 23.

(iii) $\xi=\pm i$. The presence of these two singular points is due to the factor $S(\xi)$ in the curvature operator. These singular points are irrelevant to the eigenvalue σ. These singular points are not important for the unsteady state solution, because no Stokes line, intersecting with the positive part of the real ξ axis, emanates from these points. For the sake of simplicity, therefore they are not taken into account in the present paper.

In view of the above, the whole complex ξ plane is divided into three different regions (I), (II) and (III) (see Fig. 4). In each region, the solution will have a different asymptotic expansion. The asymptotic solution obtained in this section is valid only in the outer region (I), which

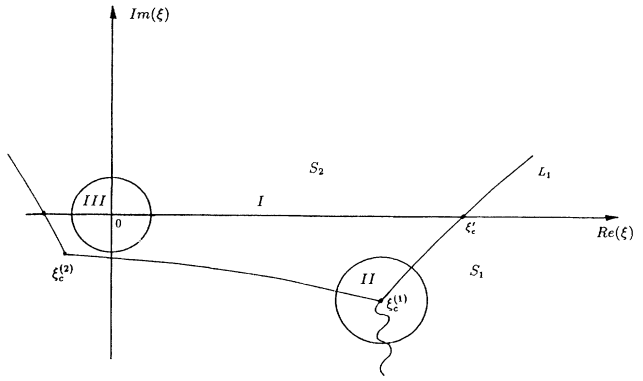

FIG. 4. Sketch of three different asymptotic expansion regions (I), (II), and (III) in the complex ξ plane.

represents two types of traveling waves. These traveling waves will interact to each other at the critical point ξ_c and the tip point $\xi=0$. The Stokes lines emanating from ξ_c divide the outer region (I) into several sectors. In particular, the Stokes line L_1 emanating from $\xi_c^{(1)}$ intersects with the real axis of ξ plane at ξ_c' and divides the real axis into two subintervals. According to the well-known Stokes phenomenon, a Wentzel-Kramers-Brillouin (WKB) type solution (4.21) will not be uniformly valid in the whole physical space ($0<\xi<\infty$). In different subintervals on the real axis, or different sectors, the coefficient pair $(D_0^{(1)},D_0^{(3)})$ will be different; their values are determined by the matching condition of the outer solution (4.21) with the inner solutions in the regions (II) and (III).

In the next section, we shall study a general type of perturbed solution, particularly the inner solution in the region (II). The singularity of turning point type at ξ_c will be explored from another approach again.

V. INNER-EXPANSION SOLUTION IN THE TURNING POINT REGION (II)

The results obtained in the preceding section indicate the existence of the critical points ξ_c in the system. In the vicinity of the point ξ_c in the complex ξ plane, the outer solution (4.2) or (4.21) is invalid. It implies that the solutions in the vicinity of ξ_c no longer have multiple scale structure. To describe such more general solutions one may use either the slow variables or the fast variables. For convenience, we utilize the fast variables (ξ_+,η_+). In doing so, the slow variables (ξ,η) in the system (3.7)–(3.12) must be changed to the fast variables through the relationship (3.5). In the following, we attempt to derive a governing equation for general perturbed interface in the limit $\epsilon\to 0$. The analysis presented below is completely independent from the normal analysis performed in Sec. IV. However, it will be seen that the results obtained through these two approaches are consistent with each other.

From (3.6), the following are derived.

1. In the liquid-state domain,

$$\left[i\frac{\partial}{\partial\xi_+}-\frac{\partial}{\partial\eta_+}\right]\tilde{T}=\epsilon\left[i\frac{\partial}{\partial\epsilon_+}+\frac{\partial}{\partial\eta_+}\right]^{-1}P\{\tilde{T}\}\ , \tag{5.1}$$

where the linear operator $P\{\tilde{T}\}$ represents all the terms inside the bracket on the right-hand side of (3.7).

2. In the solid-state domain,

$$\left[i\frac{\partial}{\partial\xi_+}+\frac{\partial}{\partial\eta_+}\right]\tilde{T}_S=\epsilon\left[i\frac{\partial}{\partial\xi_+}-\frac{\partial}{\partial\eta_+}\right]^{-1}P\{\tilde{T}_S\}\ . \tag{5.2}$$

3. On the interface: $\eta_+=0$,

$$\frac{\partial}{\partial\eta_+}(\tilde{T}-\tilde{T}_S)=i\frac{\partial}{\partial\xi_+}(\tilde{T}+\tilde{T}_S)+O(\epsilon)\ . \tag{5.3}$$

From the boundary conditions (3.8)–(3.12), one can get

$$\tilde{T}+\tilde{T}_S=\tilde{h}+\frac{2}{S}\left[\frac{d^2\tilde{h}}{d\xi_+^2}+\frac{\epsilon}{\xi}\frac{d\tilde{h}}{d\xi_+}\right]+O(\epsilon)\ ; \tag{5.4}$$

furthermore, from (3.12) and (5.3) one derives

$$i\frac{\partial}{\partial\xi_+}(\tilde{T}+\tilde{T}_s)+\sigma S^2\tilde{h}+\xi\frac{d\tilde{h}}{d\xi_+}=O(\epsilon)\ . \tag{5.5}$$

Finally from (5.4) and (5.5), letting $\epsilon\to 0$, as a leading approximation we obtain the following equation for general interface perturbations:

$$i\frac{2\epsilon^3}{S}\frac{d^3\tilde{h}_0}{d\xi_1^3}+\epsilon(\xi+i)\frac{d\tilde{h}_0}{d\xi_1}+S^2\sigma\tilde{h}_0=0\ , \tag{5.6}$$

where

$$\begin{aligned}&\xi_1=\xi-\xi_c\ ,\\ &\tilde{h}(\xi_1)=[\tilde{h}_0(\xi_1)+\epsilon\tilde{h}_1(\xi_1)+\cdots]e^{\sigma t_+/\eta_0^2}\ .\end{aligned} \tag{5.7}$$

The basic governing equation (5.6) for general interface perturbations has a great significance. From here, one may regain the local dispersion formula (4.14), by seeking for WKB types of solutions for this third-order ordinary differential equation in the outer region. To solve the general interface equation (5.6) in the vicinity of the critical point ξ_c, we introduce a transformed variable

$$\tilde{h}_0=W(\xi_1)\exp\left[\frac{i}{\epsilon}\int_{\xi_c}^{\xi}k_c(\xi_1)d\xi_1\right]\ , \tag{5.8}$$

where the reference wave-number function $k_c(\xi)$ is to be determined. Moreover, we define a differential operator

$$\frac{D}{D\xi}=\left[\frac{d}{d\xi}-\frac{ik_c}{\epsilon}\right]\ . \tag{5.9}$$

It is easy to verify that

$$\frac{D^n\tilde{h}}{D\xi^n}=\frac{d^nW}{d\xi^n}\exp\left[\frac{i}{\epsilon}\int_{\xi_c}^{\xi}k_c(\xi_1)d\xi_1\right]\ . \tag{5.10}$$

Thus, one can derive that

$$\begin{aligned}&\epsilon^3\Omega_3\frac{d^3W}{d\xi^3}+i\epsilon^2\Omega_2\frac{d^2W}{d\xi^2}\\ &\qquad-\epsilon\Omega_1\frac{dW}{d\xi}+iS^2[\sigma-\Sigma(k_c,\xi)]W=0\ ,\end{aligned} \tag{5.11}$$

where

$$\begin{aligned}\Omega_3&=\frac{1}{3!}\left[\frac{\partial^3(\Sigma S^2)}{\partial k_0^3}\right]_{k_0=k_c}=-\frac{2}{S}\ ,\\ \Omega_2&=\frac{1}{2!}\left[\frac{\partial^2(\Sigma S^2)}{\partial k_0^2}\right]_{k_0=k_c}=-\frac{6k_0}{S}\ ,\\ \Omega_1&=\left[\frac{\partial(\Sigma S^2)}{\partial k_0}\right]_{k_0=k_c}=(1-i\xi)-\frac{6k_0^2}{S}\ .\end{aligned} \tag{5.12}$$

For any given ξ, one may properly choose k_c such that

$$\left[\frac{\partial(\Sigma S^2)}{\partial k_0}\right]_{k_0=k_c}=0\ . \tag{5.13}$$

This leads to

$$k_c(\xi)=\left[\frac{S}{6}(1-i\xi)\right]^{1/2} \quad [\mathrm{Re}(k_c)>0] \ . \tag{5.14}$$

Accordingly,

$$\Sigma(k_c,\xi)=\Sigma_c(\xi)=\left[\frac{2}{27}\right]^{1/2}\left[\frac{1-i\xi}{S}\right]^{3/2} \ . \tag{5.15}$$

In terms of (5.13), Eq. (5.11) is then reduced into

$$\epsilon^3\Omega_3\frac{d^3W}{d\xi^3}+i\epsilon^2\Omega_2\frac{d^2W}{d\xi^2}+iS^2[\sigma-\Sigma_c(\xi)]W=0 \ . \tag{5.16}$$

It is seen that for any given σ, as $\xi=\xi_c^{(i)}$, $i=(1,2,3)$,

$$\sigma-\Sigma_c(\xi)=0 \ . \tag{5.17}$$

Hence, the critical points $\xi_c^{(i)}$, $(i=1,2,3)$ are actually simple turning points of the system. For any given $\sigma=|\sigma|e^{i\theta}$, from the equation (5.17) or (4.45) one can solve:

$$\begin{aligned}
\xi_c^{(1)}&=i\left[\frac{|\sigma|^{4/3}e^{i4\theta/3}-\frac{2^{2/3}}{9}}{|\sigma|^{4/3}e^{i4\theta/3}+\frac{2^{2/3}}{9}}\right] ,\\
\xi_c^{(2)}&=i\left[\frac{|\sigma|^{4/3}e^{i(4\theta/3+8\pi/3)}+\frac{2^{2/3}}{9}}{|\sigma|^{4/3}e^{i(4\theta/3+8\pi/3)}+\frac{2^{2/3}}{9}}\right] ,\\
\xi_c^{(3)}&=i\left[\frac{|\sigma|^{4/3}e^{i(4\theta/3+16\pi/3)}-\frac{2^{2/3}}{9}}{|\sigma|^{4/3}e^{i(4\theta/3+16\pi/3)}+\frac{2^{2/3}}{9}}\right] .
\end{aligned} \tag{5.18}$$

As $\sigma\to 0$, these three critical points collapse into the point $\xi=-i$; as σ is on the semicircle γ in the complex σ plane as shown in Fig. 5, these three critical points are all on the real axis ($-\infty<\xi_c<\infty$). As the eigenvalue σ belongs to the domain Σ_2, the three critical points are all in the upper-half part of the complex ξ plane. In this case, the system has no physically acceptable, continuous solution. Thus, as a necessary condition, the eigenvalue σ must be inside the semicircle γ. This condition is called the "pattern formation condition" in Ref. 23. When the eigenvalue σ belongs to the domains Σ_A and Σ_B, the critical point $\xi_c^{(1)}$ is in the lower-half part of the complex ξ plane. This is the case of the most interest. The Stokes line in the complex ξ plane is defined as

$$\mathrm{Im}\left[\int_{\xi_c}^{\xi}(k_0^{(1)}-k_0^{(3)})d\xi_1\right]=0 \ . \tag{5.19}$$

It is verified that as σ belongs to the domain $\Sigma_A+\Sigma_B$, the only one Stokes line, L_1 intersecting with the positive part of the real ξ axis emanates from $\xi_c^{(1)}$. Evidently, for the system under consideration the critical point $\xi_c^{(1)}$ plays the vital role. Hereafter, for simplicity, $\xi_c^{(1)}$ is written as ξ_c.

In the vicinity of ξ_c, if we let

$$\xi_*=\frac{\xi_1}{\epsilon^{2/3}}, \quad q_0(\epsilon)=\epsilon^{-1/6} , \tag{5.20}$$

the solution $W(\xi_1)$ can be expanded in the form

$$W(\xi_*,\epsilon)=q_0(\epsilon)W_0(\xi_*)+q_1(\epsilon)W_1(\xi_*)+\cdots . \tag{5.21}$$

Here, one should note that [through the transformation (5.8)] the long branch wave of $\tilde{h}_0$ in (4.10) will correspond to the incoming wave of W_0, while the short wave of $\tilde{h}_0$ will correspond to the outgoing wave of W_0. Now, it is not difficult to prove that in the vicinity of ξ_c, the leading approximation $W_0(\xi_*)$ can be found from the Airy equation:

$$\frac{d^2W_0}{d\xi_*^2}+A^2\xi_*W_0=0 , \tag{5.22}$$

where

$$A=-i\left[\frac{1}{6}\left[\frac{\xi+i}{S}\right]\right]^{1/2}_{\xi=\xi_c} \quad \left[-\frac{\pi}{2}<\arg(A)<0\right] . \tag{5.23}$$

One can define a complex wave-number function k_* as

$$k_*=A\xi_*^{1/2} . \tag{5.24}$$

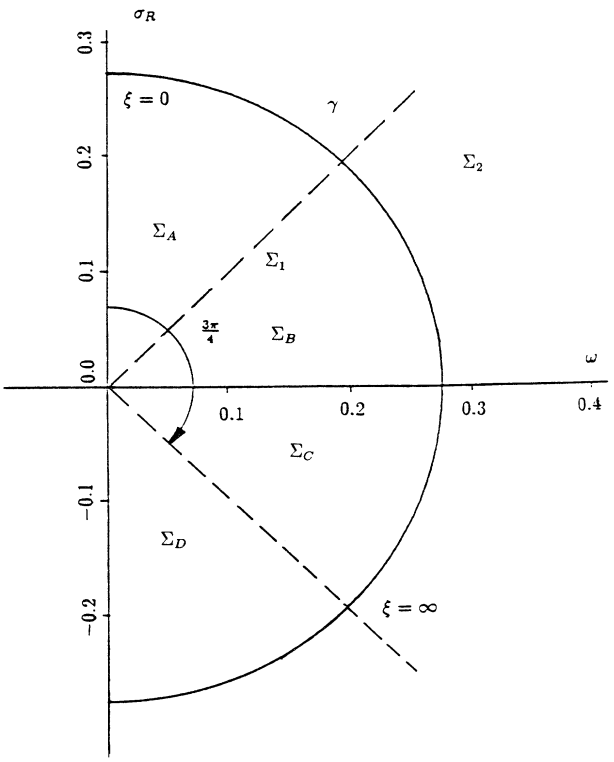

FIG. 5. As the eigenvalue σ belongs to the domain Σ_2 in the complex σ plane, the corresponding turning points ξ_c are all in the upper-half part of the complex ξ plane; while the eigenvalues σ belongs to the domain Σ_1, the corresponding turning points ξ_c are all in the lower-half part of the complex ξ plane. When the eigenvalue σ is on the curve γ, the corresponding turning points ξ_c are all on the real ξ axis.

The branch cut line in the complex ξ plane and the Stokes lines emanating from the turning point are shown in Fig. 4. To ensure the continuity of the solution, the branch cut line should not cross the real axis of ξ. Thus, it is, once more, deduced that as a necessary condition for pattern formation, the turning point ξ_c must be located in the lower half ξ plane; accordingly, the eigenvalue σ must be inside the semicircle domain Σ_1 in the complex σ plane (see Fig. 5).

The general solution of the Airy equation (5.22) (refer to Ref. 27) can be written

$$W_0(\xi_*)=C\xi_*^{1/2}H_{1/3}^{(1)}(\tfrac{2}{3}A\xi_*^{3/2})+D\xi_*^{1/2}H_{1/3}^{(2)}(\tfrac{2}{3}A\xi_*^{3/2}) . \tag{5.25}$$

When the radiation condition (3.15) in the far field is applied, one may specify the wave-number function $k_0=k_0^{(3)}$. It implies that in the far field, the solution $\tilde{h}(\xi,t)$ represents an outgoing long-wave branch; accordingly, in the sector S_1, the solution $W_0(\xi_*)$ represents an incoming wave. Consequently, one must set $C=0$, but $D\neq 0$ in the general solution (5.25). It follows that

$$W_0(\xi_*)=D\xi_*^{1/2}H_{1/3}^{(2)}(\tfrac{2}{3}A\xi_*^{3/2}) . \tag{5.26}$$

As $\mathrm{Re}(\xi_*)\to+\infty$,

$$W_0(\xi_*)\sim D_1 W_T^{(-)}(\xi_*) = D_1 e^{-i\pi/3}\frac{1}{\sqrt{k_*}}\exp\left[-i\int_0^{\xi_*}k_*\,d\xi\right] \quad (\xi_*\to+\infty) . \tag{5.27}$$

When $\mathrm{Re}(\xi_*)<0$, the solution (5.26) can be expressed as

$$W_0(\xi_*)=D_1[W_0^{(+)}(\xi_*)-e^{i\pi/3}W_0^{(-)}(\xi_*)] ; \tag{5.28}$$

as $\xi_*\to-\infty$, we have

$$W_0^{(+)}(\xi_*)\sim\frac{1}{\sqrt{k_*}}\exp\left[i\int_0^{\xi_*}k_*\,d\xi\right] \quad \text{(outgoing wave)} ,$$
$$W_0^{(-)}(\xi_*)\sim\frac{1}{\sqrt{k_*}}\exp\left[-i\int_0^{\xi_*}k_*\,d\xi\right] \quad \text{(incoming wave)} , \tag{5.29}$$

$\mathrm{Re}(k_*)>0$.

In the formulas (5.27) and (5.28), D_1 is an arbitrary constant. By matching the above turning point solution (5.26) with the outer solution, it is derived that in the sector S_1, as $\xi_c'<\xi<\infty$, where ξ_c' is the intersection point of the Stokes line L_1 with the real axis of ξ, the outer solution is

$$\tilde{h}\sim D_1 e^{-i\pi/3}\exp\left[\sigma t_{++}+\frac{i}{\epsilon}\int_{\xi_c}^{\xi}(k_0^{(3)}(\xi_1)+\cdots)d\xi_1\right]+\cdots . \tag{5.30}$$

The radiation condition in the far field is evidently satisfied. On the other hand, the coefficient pair $(D_0^{(1)},D_0^{(3)})$ of the outer solution (4.21) in the sector S_2 is derived by matching the turning point solution (5.28) with the outer solution in the sector S_2. The result is as follows:

$$\frac{D_0^{(3)}}{D_0^{(1)}}=e^{i\chi_*} , \tag{5.31}$$

where

$$\chi_*=(2n-\tfrac{2}{3})\pi+\frac{1}{\epsilon}\int_0^{\xi_c}(k_0^{(1)}-k_0^{(3)})d\xi \quad (n=0,\pm1,\pm2,\pm3,\ldots) . \tag{5.32}$$

To obtain the global-mode solution in the whole physical region ($0\le\xi<\infty$), one must also satisfy the tip smoothness condition. For this purpose, one must find the inner solution in the tip region (III) where $\xi=O(\epsilon)$ and match it with the outer solution in the intermediate region. This matching condition will result in a quantum condition for the eigenvalues σ of each mode.

VI. INNER-EXPANSION SOLUTION IN THE TIP REGION (III)

As $\xi\to0$, the MVE (4.2) is no longer valid, because the two terms

$$\frac{\partial^2\tilde{T}}{\partial\xi_+^2} \quad \frac{\epsilon}{\xi}\frac{\partial\tilde{T}}{\partial\xi_+} \tag{6.1}$$

in the governing equation (3.7) are the same order of magnitude. In order to find the inner solution in the tip region (III), one has to use a single length scale and the following system:

$$\left[\frac{\partial^2}{\partial\xi_+^2}+\frac{\partial^2}{\partial\eta_+^2}+\frac{1}{\xi_+}\frac{\partial}{\partial\xi_+}\right]\tilde{T} = \epsilon\left[-\frac{1}{\eta}\frac{\partial\tilde{T}}{\partial\eta_+}+\eta_0^4(\xi^2+\eta^2)\frac{\partial\tilde{T}}{\partial t_+} +\eta_0^2\left[\xi\frac{\partial\tilde{T}}{\partial\xi_+}-\eta\frac{\partial\tilde{T}}{\partial\eta_+}\right]\right] . \tag{6.2}$$

The boundary conditions (3.8)–(3.12) are still valid, except the condition (3.11) must be replaced by the following:

$$\tilde{T}_S=\frac{1}{S(\xi)}\left[\frac{\partial^2\tilde{h}}{\partial\xi_+^2}+\frac{1}{\xi_+}\frac{\partial\tilde{h}}{\partial\xi_+}+\frac{\epsilon\xi}{S^2(\xi)}\frac{\partial\tilde{h}}{\partial\xi_+}-\frac{\epsilon^2}{S^2(\xi)}\tilde{h}\right]. \tag{6.3}$$

Keep in mind that in the above system,

$$\xi=\epsilon\xi_+;\quad \eta=1+\epsilon\eta_+ . \tag{6.4}$$

To derive the tip solution, one needs to use the tip fast variables in the form (not to be confused with the fast variables ξ_{++} and η_{++} in the outer region)

$$\begin{aligned}&\xi_{++}=\hat{k}\xi_+ ,\\ &\eta_{++}=\hat{k}\eta_+ ,\\ &t_{++}=t_+/\eta_0^2 .\end{aligned} \tag{6.5}$$

Consider the following inner-expansion solution:

$$\begin{aligned}&\tilde{T}=[\mu_0(\epsilon)\tilde{T}_0+\mu_1(\epsilon)\tilde{T}_1+\cdots]e^{\sigma t_+/\eta_0^2},\\ &\tilde{T}_S=[\mu_0(\epsilon)\tilde{T}_{S0}+\mu_1(\epsilon)\tilde{T}_{S1}+\cdots]e^{\sigma t_+/\eta_0^2},\\ &\tilde{h}=[\mu_0(\epsilon)\tilde{h}_0+\mu_1(\epsilon)\tilde{h}_1+\cdots]e^{\sigma t_+/\eta_0^2},\\ &\hat{k}=\hat{k}_0+\epsilon\hat{k}_1+\epsilon^2\hat{k}_2+\cdots .\end{aligned} \tag{6.6}$$

By substituting the above expansions into the equation (6.2) and the corresponding boundary conditions, one can find each order approximate solution, successively. The results for the zeroth-order approximation $[O(\mu_0(\epsilon))]$ are as follows:

$$\begin{aligned}&\frac{\partial^2\tilde{T}_0}{\partial\xi_{++}^2}+\frac{\partial^2\tilde{T}_0}{\partial\eta_{++}^2}+\frac{1}{\xi_{++}}\frac{\partial\tilde{T}_0}{\partial\xi_{++}}=0 ,\\ &\frac{\partial^2\tilde{T}_{S0}}{\partial\xi_{++}^2}+\frac{\partial^2\tilde{T}_{S0}}{\partial\eta_{++}^2}+\frac{1}{\xi_{++}}\frac{\partial\tilde{T}_{S0}}{\partial\xi_{++}}=0 ;\end{aligned} \tag{6.7}$$

the boundary conditions at $\eta_{++}=0$ are

$$(1)\ \tilde{T}_0=\tilde{T}_{S0}+\tilde{h}_0 , \tag{6.8}$$

$$(2)\ \tilde{T}_{S0}=\hat{k}_0^2\left[\frac{\partial^2\tilde{h}_0}{\partial\xi_{++}^2}+\frac{1}{\xi_{++}}\frac{\partial\tilde{h}_0}{\partial\xi_{++}}\right], \tag{6.9}$$

$$(3)\ \hat{k}_0\frac{\partial}{\partial\eta_{++}}(\tilde{T}_0-\tilde{T}_{S0})+\sigma\tilde{h}_0=0 . \tag{6.10}$$

The general solution of (6.7) is

$$\begin{aligned}&\tilde{T}_0=a_0H_0^{(i)}(\xi_{++})e^{-\eta_{++}},\\ &\tilde{T}_{S0}=a_{S0}H_0^{(i)}(\xi_{++})e^{\eta_{++}}\quad(i=1,2)\end{aligned} \tag{6.11}$$

where a_0 and a_{S0} are arbitrary constants, $H_0^{(1),(2)}(\xi_{++})$ are the Hankel functions of first and second kind. It is seen from matching condition with the outer solution that, one can only choose $H_0^{(i)}(\xi_{++})=H_0^{(1)}(\xi_{++})$. Furthermore, setting

$$\tilde{h}_0=d_0H_0^{(1)}(\xi_{++}) , \tag{6.12}$$

from the boundary conditions (6.8)–(6.10), it is obtained that

$$\begin{aligned}&a_0=(1-\hat{k}_0^2)d_0 ,\\ &a_{S0}=-\hat{k}_0^2d_0 ,\end{aligned} \tag{6.13}$$

where $\hat{k}_0$ satisfies the dispersion relationship

$$\sigma=\hat{k}_0(1-2\hat{k}_0^2) . \tag{6.14}$$

From the equation (6.14), one can find three roots. By comparing (6.14) with the local dispersion formula (4.14), these roots can be written as

$$\begin{aligned}&\hat{k}_0^{(1)}=k_0^{(1)}(0) ,\\ &\hat{k}_0^{(2)}=k_0^{(2)}(0) ,\\ &\hat{k}_0^{(3)}=k_0^{(3)}(0) .\end{aligned} \tag{6.15}$$

The root $\hat{k}_0^{(2)}$ is ruled out due to $\mathrm{Re}(\hat{k}_0^{(2)})<0$. Therefore, the general solution of $\tilde{h}_0$ in the tip region (III) is

$$\tilde{h}_0=d_0^{(1)}H_0^{(1)}(\hat{k}_0^{(1)}\xi_+)+d_0^{(3)}H_0^{(1)}(\hat{k}_0^{(3)}\xi_+) . \tag{6.16}$$

To satisfy the tip smoothness condition (2.23), one must set

$$d_0^{(1)}+d_0^{(3)}=0 . \tag{6.17}$$

Thus, the tip solution in region (III) is derived as

$$\tilde{h}_0=d_0[H_0^{(1)}(\hat{k}_0^{(1)}\xi_+)-H_0^{(1)}(\hat{k}_0^{(3)}\xi_+)] . \tag{6.18}$$

As $\xi_{++}\to\infty$, the tip solution behaves as

$$\tilde{h}\approx d_0e^{\sigma t_{++}}\left[\frac{1}{[k_0^{(1)}(0)\xi_+]^{1/2}}e^{ik_0^{(1)}(0)\xi_+}-\frac{1}{[k_0^{(3)}(0)\xi_+]^{1/2}}e^{ik_0^{(3)}(0)\xi_+}\right] . \tag{6.19}$$

One may apply the transformation (5.8) to the tip solution or (6.19). Then (6.19) can be rewritten in the form

$$\tilde{h}\approx d_0\exp[\sigma t_{++}+k_c(0)\xi_+]\times\left[\left[\frac{\Delta k_0^{(1)}}{k_0^{(1)}(0)}\right]^{1/2}W_0^{(+)}-\left[\frac{\Delta k_0^{(3)}}{k_0^{(3)}(0)}\right]^{1/2}W_0^{(-)}\right] , \tag{6.20}$$

where

$$\begin{aligned}&W_0^{(+)}=\frac{1}{(\Delta k_0^{(1)}\xi_+)^{1/2}}e^{i\Delta k_0^{(1)}\xi_+} ,\\ &W_0^{(-)}=\frac{1}{(\Delta k_0^{(3)}\xi_+)^{1/2}}e^{i\Delta k_0^{(3)}\xi_+} ,\\ &\Delta k_0^{(1)}=k_0^{(1)}(0)-k_c(0) ,\\ &\Delta k_0^{(3)}=k_0^{(3)}(0)-k_c(0) .\end{aligned} \tag{6.21}$$

The formula (6.20) gives a physical interpretation to the tip solution. As an incoming wave $W_0^{(-)}$ reaches the leading edge of the tip, it is reflected, and transformed to an outgoing wave $W_0^{(+)}$ as shown in Fig. 6. We call this process the signal feed-back mechanism.

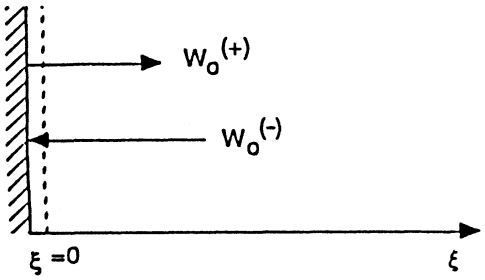

FIG. 6. Sketch of the signal feedback process near the leading edge of the tip.

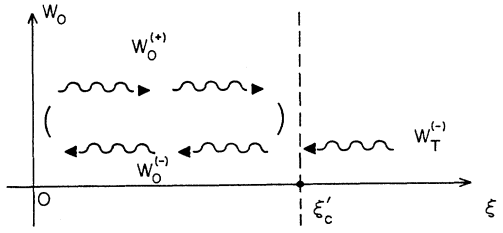

FIG. 7. The wave diagram of the GTW mode.

VII. GLOBAL TRAPPED WAVE MODE AND ITS QUANTUM CONDITION

We can match the tip solution (6.19) [or (6.20)] with the outer solution (4.43) in the intermediate region in sector S_2. This will end at the desired uniformly valid global-mode solutions. The matching condition leads to

$$\mu_0(\epsilon)=\epsilon^{-1/2} \tag{7.1}$$

and

$$D_0^{(1)}=\frac{d_0}{(k_0^{(1)}(0))^{1/2}}\ ,$$
$$D_0^{(3)}=-\frac{d_0}{(k_0^{(3)}(0))^{1/2}}\ , \tag{7.2}$$

so that

$$\frac{D_0^{(1)}}{D_0^{(3)}}=-\left[\frac{k_0^{(3)}(0)}{k_0^{(1)}(0)}\right]^{1/2}\ . \tag{7.3}$$

From (7.3) and (5.31), it is seen that as far as the global mode is concerned, in order for the outer solution in the sector S_2 to match with both the turning point solution (5.26) and the tip solution (6.19) [or (6.20)], the phase condition

$$e^{i\chi_*}=-\left[\frac{k_0^{(1)}(0)}{k_0^{(3)}(0)}\right]^{1/2} \tag{7.4}$$

must be satisfied. This leads to the quantum condition of the mode

$$\frac{1}{\epsilon}\int_0^{\xi_c}(k_0^{(1)}-k_0^{(3)})d\xi=(2n+1+\tfrac{2}{3}+\frac{\theta_0}{2})\pi-\frac{i}{2}\ln\alpha_0\ ,$$
$$n=(0,\pm1,\pm2,\pm3,\ldots)\ , \tag{7.5}$$

where

$$\alpha_0 e^{i\theta_0\pi}=k_0^{(1)}(0)/k_0^{(3)}(0)\ . \tag{7.6}$$

For any given small parameter ϵ, the above quantum condition determines a discrete set of the complex eigenvalues $\{\sigma_n\}$ $(n=0,1,2,\ldots)$ and the corresponding global modes. Only a finite number of growing unstable modes is possible. Table I lists the eigenvalues of the first four modes for $\epsilon=0.1$. As $\epsilon\to0$, the eigenvalue of the fastest growing mode corresponding to $n=0$, apparently tends to the limit $\sigma=(0.2722,0.0)$, which corresponds to the maximum growth rate of the Mullins-Sekerka instability.

The global-mode solutions that are obtained in the present section have, we believe, an important physical significance. A wave diagram for these global modes is sketched in Fig. 7. It is seen that an incident outgoing wave $W_0^{(+)}$ from the tip collides with an incoming wave from the far field at the point ξ_c' on the Stokes line L_1; the collision generates an incoming wave $W_0^{(-)}$ towards to the tip region. This incoming wave $W_0^{(-)}$ is then reflected at the tip region, and becomes an outgoing wave $W_0^{(+)}$ again. The waves appears trapped in the sector S_2 between the tip point and the point ξ_c'. No wave escapes outside the Stokes line L_1. For this reason, we call these global modes global trapped wave (GTW) modes. In the far field the solution $\tilde{h}(\xi,t)$ describes a long outgoing wave.

VIII. GLOBAL WEASR MODES AND PERTURBED INTERFACIAL ENERGY CONDITION

The global trapped wave mode obtained in the previous section is not the only type of global mode that the system may have. One may also set the wave number function k_0 in the radiation condition (3.15) be the wave number $k_0^{(1)}$. This implies that in the far field, the solution $\tilde{h}(\xi,t)$ represents a short outgoing wave instead of a long outgoing wave, the solution W represents an outgoing wave. Details of this solution will not be presented here. Figure 8 indicates the pattern of these waves. We

TABLE I. GTW mode; $\epsilon=0.1$

n	ξ_c	σ
0	$(0.1147\times10,-0.4944)$	$(0.4246\times10^{-1},-0.1959)$
1	$(0.2053\times10,-0.5835)$	$(-0.3292\times10^{-1},-0.2296)$
2	$(0.2823\times10,-0.6196)$	$(-0.7145\times10^{-1},-0.2357)$
3	$(0.4155\times10,-0.6498)$	$(-0.9450\times10^{-1},-0.2356)$

call this process, the WEASR (wave emission at the turning point and signal reflections between the turning point and the tip) mechanism.

Table II lists the eigenvalues of the first four WEASR modes for $\epsilon=0.1$. Figure 9 shows the variation of growth rate of GTW mode ($n=0$) and WEASR mode ($n=0$) with the parameter ϵ, while Fig. 10 shows the variation of the frequency of these modes with ϵ. It is clearly seen that the surface tension suppresses the global instabilities, as expected. Note that in the far field, the outer solution (5.30) can be expressed in the form

$$\tilde{h}_0 \sim A(\xi,t)e^{i\phi(\xi,t)/\epsilon}, \tag{8.1}$$

where

$$\Phi(\xi,t)=\int_{\xi_c}^{\xi}\mathrm{Re}(k_0)d\xi-\frac{\omega t}{\eta_0^2}, \tag{8.2}$$

$$A(\xi,t)=\exp\left[\frac{\sigma_R t}{\epsilon\eta_0^2}-\frac{1}{\epsilon}\int_{\xi_c}^{\xi}\mathrm{Im}(k_0)d\xi\right]. \tag{8.3}$$

As $\xi\to\infty$, for any fixed eigenvalue σ, the wave functions $k_0^{(i)}$. ($i=1,2,3$) have the asymptotic expansion

$$k_0^{(i)}(\xi)\sim a_0^{(i)}\xi+a_1^{(i)}+\frac{a_2^{(i)}}{\xi}+\cdots. \tag{8.4}$$

The phase velocity of the wave along the interface $\eta=1$ is

$$V_p=-\left[\frac{\partial\Phi}{\partial t}\right]\Big/\left[\frac{\partial\Phi}{\partial l}\right]=\frac{\omega(1+\xi^2)^{1/2}}{\mathrm{Re}[k_0(\xi)]}; \tag{8.5}$$

in the far field

$$V_p\approx\frac{\omega}{\mathrm{Re}(a_0)}\quad(\xi\to\infty). \tag{8.6}$$

Moreover, one can define the function

$$P(t)=\int_0^{\infty}|A(\xi_1,t)|^2d\xi_1, \tag{8.7}$$

which measures the total perturbed interfacial energy. From physical consideration, the total perturbed interfacial energy function $P(t)$ must be finite. It is seen that the total perturbed interfacial energy function $P(t)$ for WEASR modes is infinite because $\mathrm{Im}(a_0)<0$ for all $\epsilon>0$ (see Fig. 12). Therefore, WEASR modes are not physically meaningful for the free dendrite growth problem. It can also be seen that the phase velocity of wave along the interface is

(1) for the GTW modes,

$$V_p(\infty)\approx 1.0; \tag{8.8}$$

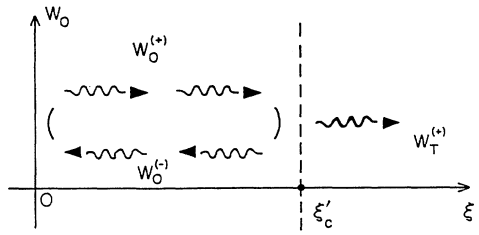

FIG. 8. The wave diagram of the WEASR mode.

(2) for the WEASR modes,

$$V_p(\infty)\approx 0.05-0.5 \tag{8.9}$$

(see Fig. 11). The result (8.8) shows that in the far field, the phase velocity of wave V_p of GTW modes in a coordinate system moving with the dendrite tip approximately equals to the tip velocity in the laboratory frame. This result agrees well with experimental observations.

IX. PATTERN FORMATION AND SELECTION OF TIP VELOCITY

The existence of growing GTW modes explains the origin and essence of the dendritic structure in the solidifying system. Any initial perturbation in the growth process will stimulate a spectrum of the above global modes. As $t\to\infty$, all decaying modes will vanish, while the amplitudes of the growing modes exponentially increase. Eventually, the GTW mode with the largest growth rate dominates the feature of the microstructure of dendrite. From the GTW mechanism, one can see that to form a pattern in solidification, the conditions both at the tip and at the root are important. In linear instability theory, the amplitude of a growing mode exponentially increases as the time passes. In the real system, however, one can anticipate that when the amplitude becomes large, its further increase would be suppressed by nonlinearity and other dissipative effects that may be involved. Eventually, it appears that with GTW mode the head of dendrite persistently emits a long interfacial wave train propagating along the interface toward the far field with a phase velocity of nearly unity. This forms the fantastic pattern that was observed in experiments (see Fig. 1).

A significant question is thus raised: Among all the GTW modes, which one is naturally selected in a realistic dendrite? Our answer to this question is that the selected GTW mode is near the neutral point of linear stability. The reason is that the realistic dendrite at the later growth stage should be in a nonlinear neutrally stable

TABLE II. WEASR mode; $\epsilon=0.1$

n	ξ_c	σ
0	$(0.6860,-0.4078)$	$(0.9997E\times10^{-1},-0.1504)$
1	$(0.1697\times10,-0.5571)$	$(-0.8260\times10^{-2},-0.2217)$
2	$(0.2514\times10,-0.6077)$	$(-0.5800\times10^{-1},-0.2344)$
3	$(0.3235\times10,-0.6319)$	$(-0.8614\times10^{-2},-0.2360)$

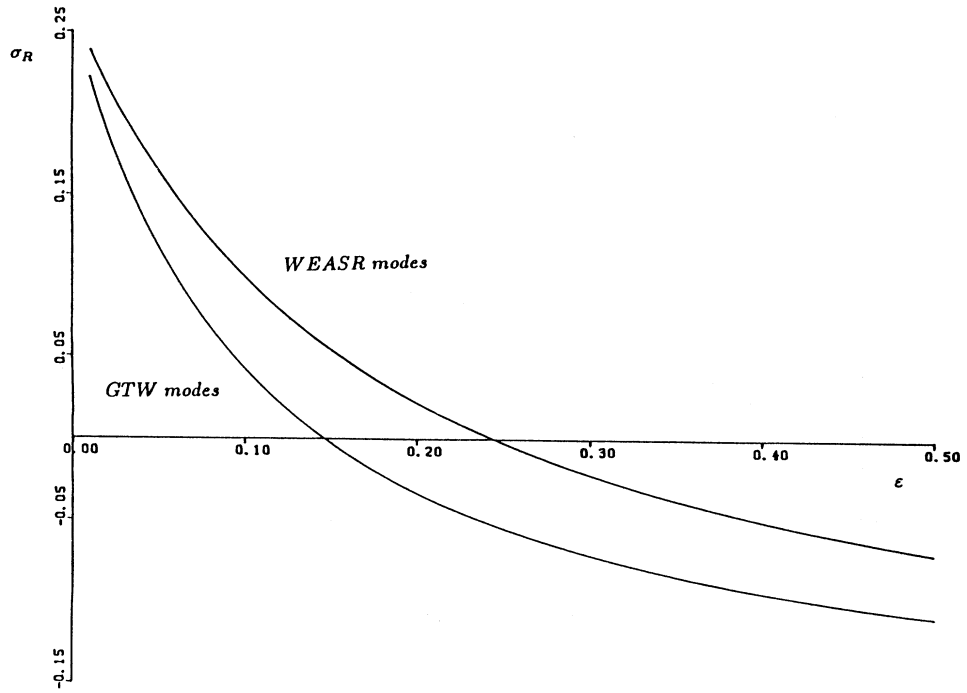

FIG. 9. The variation of growth rate of GTW and WEASR modes vs ϵ.

state. The nonlinear neutrally stable perturbed state is determined by nonlinear bifurcation theory. This state, however, in linear stability must be a weakly growing mode. It is near the neutral point of linear stability. This important conclusion is verified by experimental evidence, since one sees that in the frame moving with the tip, the whole dendritic growth process at the later stage, is indeed in a nonlinear neutrally stable state. The amplitude of oscillation at any point on the interface is apparently time independent. It is the entire interface that is neutrally stable, not just the dendrite tip. We call the above-mentioned neutrally stable state for the entire interface the global neutrally stable (GNS) state. This GNS state is determined by the condition for the GTW mode ($n=0$):

$$\sigma_R(\epsilon_*)=0 \ . \tag{9.1}$$

The eigenfunction $\tilde{h}_0(\xi)$ of the global neutrally stable state for the case $T_\infty=-0.068\,44$, $\eta_0=0.2$ is shown in Fig. 13, while the corresponding interface shape of the dendrite is shown in Fig. 14. The value of ϵ_* is found to be

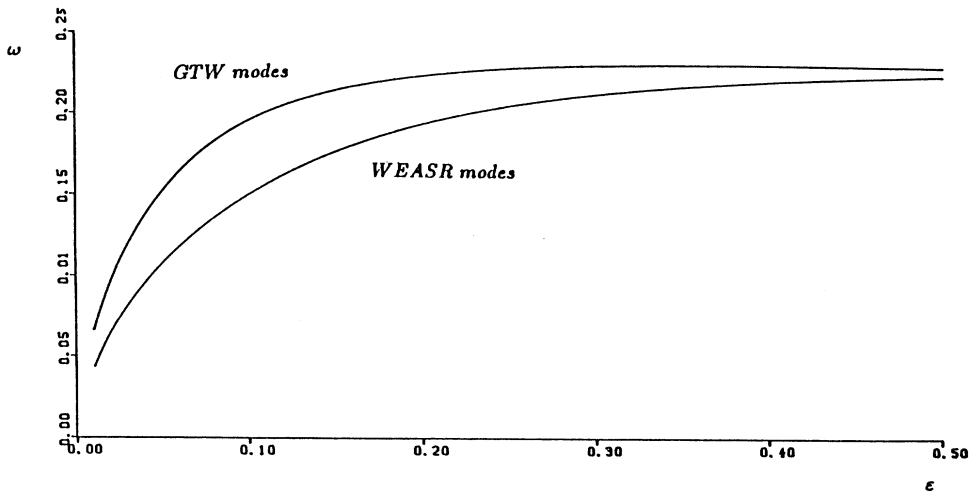

FIG. 10. The variation of frequency of GTW and WEASR modes vs ϵ.

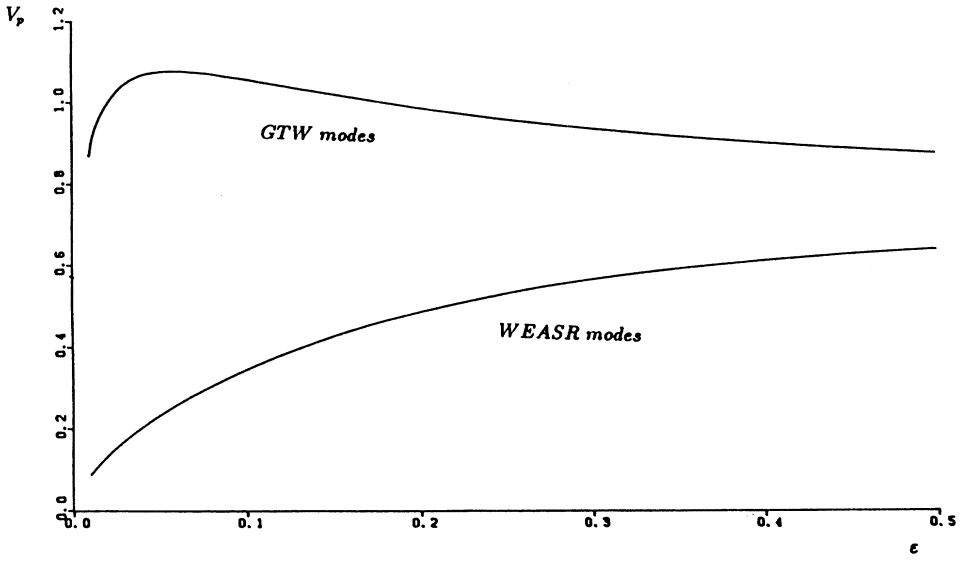

FIG. 11. The variation of phase velocity V_p of GTW and WEASR modes in the far field vs ϵ.

$$\epsilon_* = \left[\frac{l_c \kappa_T}{U l_b^2} \right]^{1/2} = 0.1470 \ . \tag{9.2}$$

From this value we can calculate the velocity of the dendrite tip. We call the condition (9.1) the global neutral stability (GNS) condition for the selection of growth velocity. In the literature, some authors used Langer's stability parameter σ_*. The relation between the parameter ϵ_* and σ_* is

$$\epsilon_* = \left[\frac{\sigma_*}{2} \right]^{1/2} \ . \tag{9.3}$$

The phase velocity of the above selected GTW mode in the far field is found to be

$$V_p \approx 1.02 \quad (\text{as } \xi \to \infty) \ . \tag{9.4}$$

Experimental data for succinonitrile with the anisotropy $\epsilon_4 = 0.005$ show that (see Ref. 29)

$$(\epsilon_*)_{\text{exp}} = 0.099 \ . \tag{9.5}$$

It is seen that the GNS condition (9.1) is in a reasonably good agreement with the available experimental data. The difference between the theoretical value and the experimental data in ϵ_* is about a factor $\sqrt{2}$. It is also seen

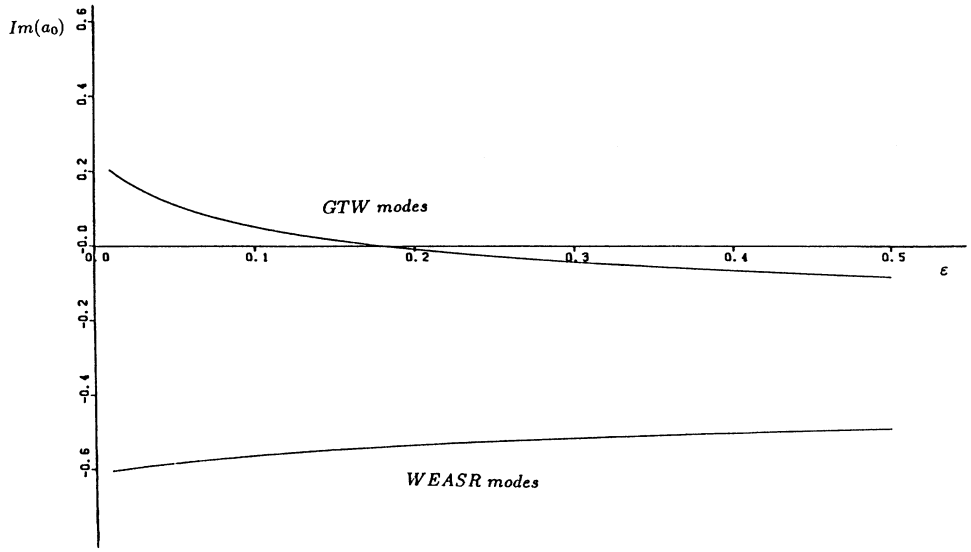

FIG. 12. The variation of the coefficient of amplitude function in the far field, $\text{Im}(a_0)$ vs ϵ.

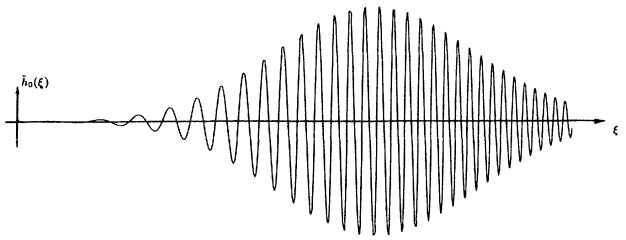

FIG. 13. The eigenfunction $\tilde{h}_0(\xi)$ of the global neutral stable state for the case $\epsilon=\epsilon_*$, $n=0$, $T_\infty=-0.068\,44$, $\eta_0=0.2$.

from Fig. 14 and the result (9.4) that the predictions of the present theory to the interface shape of a growing dendrite and the phase velocity V_p are qualitatively in good agreement with the experimental observations. The zeros of the GNS mode solution $\tilde{h}_0(\xi)$ for the case $T_\infty=-0.068\,44$ in the outer region ($\xi_c'=2.36<\xi<\infty$) are computed. If one uses the arc length l starting from $\xi=0$ along the paraboloid $\eta=1$ as the independent variable, then at the zeros

$$\left\{\frac{l_n}{l_b}\right\}=3.32;4.03;4.62;5.14;5.62;6.05;6.47;\ldots. \quad (9.6)$$

From these numbers, one can easily calculate the arc length $\{\lambda_n\}$ between the two adjacent zeros along the paraboloid $\eta=1$, which may represent the half-wave lengths of the GNS mode along the paraboloid $\eta=1$ and measured by the tip radius l_b. We obtain that

$$\{\lambda_n\}=0.71;0.59;0.48;0.43;0.42;\ldots. \quad (9.7)$$

The precise, experimental measurements for these quantities, however, have not been seen yet.

The discrepancy between the present theory and the experimental data can be explained as that besides the surface tension, the system also has some other stabilizing effects neglected by the present theory. These stabilizing effects may be considered to come from two main sources: (1) the effect of higher-order nonlinearity, since the present linear theory is only concerned with the leading approximation. (2) the effects of the physical parameters neglected by this theory, such as the anisotropy of surface tension, the fluid motion due to the density change during the phase transition, the difference of the thermodynamical constants between the liquid and the solid state, etc.

The influence of these effects on the value of the parameter ϵ_* and the global stability of the system is a significant problem which can be studied by extending the method developed in this work. Finally, it should be pointed out that the global instability mechanism for another important pattern formation problem—the viscous fingering in Hele-Shaw cell—can be also explored by following the same idea addressed in the present paper. This widely concerned subject is currently under our investigation. The results will be published elsewhere (see Ref. 30).

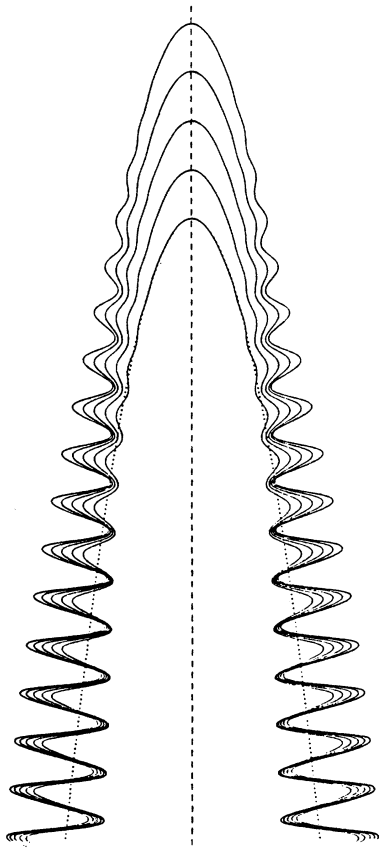

FIG. 14. The interface shape of dendrite in the global neutrally stable state for the case $n=0$, $T_\infty=-0.068\,44$, $\eta_0=0.2$.

X. SUMMARY

The present work deals with the global instability mechanism in solidification. It interprets the origin and essence of the dendritic structure of a growing needle crystal with arbitrary undercooling and gives a solution to the selection of tip velocity. The dendrite growth process is formulated as a linear eigenvalue problem. The major conclusions drawn are summarized as follows.

1. The dendrite growth is intrinsically a time-dependent wave phenomenon for the case of nonzero surface tension. The solution for a realistic dendrite growth is not the stable, steady state near the Ivantsov solution, but it is the time-dependent global neutrally stable state near the Ivantsov solution.

2. Anisotropy of surface tension is not a necessary condition for dendrite growth. A selection condition of the tip velocity is found even in the isotropic case.

3. The normal-mode perturbations are subject to a local dispersion relation (3.15). This formula is a generalization of the Mullins-Sekerka dispersion formula to a more general solidification system, whose local growth velocity of the interface not only has a normal component but also a tangential component.

4. A higher-order approximation to the normal-mode solution proves the existence of a special simple turning point ξ_c, which is related to the eigenvalue σ of the unsteady solution. The location of this turning point ξ_c in

the complex ξ plane must be below the real axis; or say, the eigenvalue σ must belong to the domain Σ_1 in the complex σ plane, as shown in Fig. 5. This necessary condition is called the "pattern formation condition."[23]

5. The presence of the above-mentioned special simple turning point ξ_c plays a vital role for the pattern formation and the selection of tip velocity. In order to obtain the global-mode solutions for dendritic growth, one must impose the radiation condition in the far field and the smooth condition at the tip of dendrite.

6. The global instability mechanism of the dendrite growth system is an entirely new instability mechanism generated by the turning point ξ_c. It is determined by the wave interactions at the turning point and the leading edge of the tip. We have found two types of global instability mechanisms in the system: the GTW mechanism and the WEASR mechanism, which generate two different discrete sets of global wave modes. In the far field, the amplitude of the growing GTW mode vanishes and its phase speed is nearly the unity; also in the far field, the amplitude of the WEASR mode exponentially increases, and its phase speed is rather small. The physical requirement that the total perturbed interfacial energy must be finite rules out all the WEASR modes. The presence of self-sustaining GTW modes connects to the dynamics of dendritic pattern formation on a growing needle crystal.

7. The system allows a unique global neutral stable GTW mode, and satisfies the requirement that the total perturbed energy of the system is finite. It is proposed that at the later stage, the dendrite growth is in the global neutrally stable state, so that the global neutral stability condition selects the tip velocity of the dendrite. This condition determines the value of the stability parameter $\epsilon_* = 0.1470$, which is in reasonably good agreement with experimental data.

ACKNOWLEDGMENTS

The author is deeply grateful to Dr. J. D. Cole for his invaluable input and constant discussion; he also thanks Professor Pan Zhong-Xiong very much for his assistance in part of the numerical computations. This research was supported by the Operating Grants of Natural Sciences and Engineering Research Council of Canada (NSERC). Partial funding was also provided by the Canadian Space Agency under Contract No. 04SW. 31016-9-6056.

APPENDIX

The system for the perturbed state with the multiple variables is listed as follows:

$$k^2\left[\frac{\partial^2}{\partial\xi_{++}^2}+\frac{\partial^2}{\partial\eta_{++}^2}\right]\tilde{T}=\epsilon\eta_0^2(\xi^2+\eta^2)\frac{\partial\tilde{T}}{\partial t_{++}}+\epsilon\eta_0^2\xi\left[k\frac{\partial}{\partial\xi_{++}}+\epsilon\frac{\partial}{\partial\xi}\right]\tilde{T}-\epsilon\eta_0^2\eta\left[k\frac{\partial}{\partial\eta_{++}}+\epsilon\frac{\partial}{\partial\eta}\right]\tilde{T}$$
$$-\frac{\epsilon}{\xi}\left[k\frac{\partial}{\partial\xi_{++}}+\epsilon\frac{\partial}{\partial\xi}\right]\tilde{T}-\frac{\epsilon}{\eta}\left[k\frac{\partial}{\partial\eta_{++}}+\epsilon\frac{\partial}{\partial\eta}\right]\tilde{T}$$
$$-\epsilon\left[2k\frac{\partial^2}{\partial\xi\partial\xi_{++}}+2k\frac{\partial^2}{\partial\eta\partial\eta_{++}}+\frac{\partial k}{\partial\xi}\frac{\partial}{\partial\xi_{++}}\right]\tilde{T}-\epsilon^2\left[\frac{\partial^2}{\partial\xi^2}+\frac{\partial^2}{\partial\eta^2}\right]\tilde{T}\ . \tag{A1}$$

The boundary conditions are the following:

(1) As $\eta_{++}\to\infty$, $\tilde{T}\to 0$; (A2)

(2) As $\eta_{++}\to 0$, $\tilde{T}_S\to 0$; (A3)

(3) On the interface $\eta_{++}=0$, $\eta=1$,

(i) The thermodynamic equilibrium condition applies:

$$\tilde{T}=\tilde{T}_S+\tilde{h}+O(\epsilon)\ . \tag{A4}$$

(ii) The Gibbs-Thomson condition applies:

$$\tilde{T}=\frac{1}{S(\xi)}\left[\left[k^2\frac{\partial^2}{\partial\xi_{++}^2}+2\epsilon k\frac{\partial^2}{\partial\xi_{++}\partial\xi}+\epsilon\frac{\partial k}{\partial\xi}\frac{\partial}{\partial\xi_{++}}+\epsilon^2\frac{\partial^2}{\partial\xi^2}\right]\right.$$
$$\left.+\epsilon\left[\frac{1}{\xi}+\frac{\xi}{S^2(\xi)}\right]\left[k\frac{\partial}{\partial\xi_{++}}+\epsilon\frac{\partial}{\partial\xi}\right]-\frac{\epsilon^2}{S^2(\xi)}\right]\tilde{h}+O(\epsilon^3)\ . \tag{A5}$$

(iii) The heat balance condition applies:

$$\left[k\frac{\partial}{\partial\eta_{++}}+\epsilon\frac{\partial}{\partial\eta}\right]\left[\tilde{T}-\tilde{T}_S\right]+S^2(\xi)\frac{\partial\tilde{h}}{\partial t_{++}}+\xi\left[k\frac{\partial}{\partial\xi_{++}}+\epsilon\frac{\partial}{\partial\xi}\right]\tilde{h}+\epsilon(2+\eta_0^2)\tilde{h}+O(\epsilon^2)=0\ . \tag{A6}$$

[1]G. P. Ivantsov, Dokl. Akad. Nauk, SSSR **58**, 567 (1947).
[2]G. Horvay and J. W. Cahn, Acta Metall. **9**, 695 (1961).
[3]J. S. Langer, Rev. Mod. Phys. **52**, 1 (1980).
[4]G. E. Nash and M. E. Glicksman, Acta Metall. **22**, 1283 (1974).
[5]J. S. Langer and H. Müller-Krumbaar, Acta Metall. 26 (1978); **26**, 1689 (1978); **26**, 1697 (1978).
[6]M. E. Glicksman, R. J. Schaefer, and J. D. Ayers, Metall. Trans. A **7**, 1747 (1976).
[7]M. E. Glicksman, R. J. Schaefer, and J. D. Ayers, Philos. Mag. **32**, 725 (1975).
[8]J. S. Langer, in *Lectures in the Theory of Pattern Formation,* Proceedings of the USMG NATO AS Les Houches Session, XLVI, 1986-Le hasard et la matiere/chance and matter, edited by J. Souletie, J. Vannimenus, and R. Stora (Elsevier, New York, 1986).
[9]D. A. Kessler and H. Levine, Phys. Rev. Lett. **57**, 3069 (1986).
[10]M. Kruskal and H. Segur (unpublished).
[11]C. Amick and B. Mcleod (private communication).
[12]J. M. Hammersley and G. Mazzarino, IMA J. Appl. Math. **42**, 43 (1989).
[13]J. J. Xu, Studies Appl. Math. **82**, 71 (1990).
[14]D. A. Kessler and H. Levine, Phys. Rev. Lett. **57**, 3069 (1986).
[15]D. Bensimon, P. Pelce, and B. I. Shraiman, J. Phys. **48**, 2081 (1987).
[16]P. Pelce and Y. Pomeau, Studies Appl. Math. **74**, 245 (1986).
[17]M. N. Barber, A. Barbieri, and J. S. Langer, Phys. Rev. **36**, 3340 (1987).
[18]J. S. Langer, Phys. Rev. A **36**, 3350 (1987).
[19]J. J. Xu, in *Structure and Dynamics of Partially Solidified System,* Vol. 125 of *NATO Advanced Study Institute, Series E: Applied Sciences,* edited by D. E. Loper (Nijhoff, Dordrecht, 1987), p. 97.
[20]J. J. Xu, Phys. Rev. A **37**, 3087 (1988).
[21]C. C. Lin and Y. Y. Lau, SIMA J. Appl. Math. **29**, 352 (1975).
[22]P. G. Drazin and W. H. Reid, *Hydrodynamic Stability* (Cambridge University Press, Cambridge, England, 1981).
[23]J. J. Xu, Phys. Rev. A **40**, 1599 (1989); **40**, 1609 (1989).
[24]J. J. Xu, Can. J. Phys. **68**, 58 (1990).
[25]J. J. Xu, Phys. Status Solidi B **157**, 577 (1990).
[26]J. J. Xu, J. Crystal Growth **100**, 481 (1990).
[27]*Handbook of Mathematical Functions,* edited by M. Abramowitz and I. A. Stegun (Dover, New York, 1964).
[28]J. Kevorkian and J. D. Cole, in *Perturbation Methods in Applied Mathematics,* Vol. 34 of *Applied Mathematical Sciences,* edited by F. John, J. E. Marsden, and L. Sirovich (Springer-Verlag, Berlin, 1981).
[29]S. C. Huang and M. E. Glicksmann, Acta Metall. **29**, 701 (1981).
[30]J. J. Xu, McGill University Report No. (90-28), Montreal, Quebec, Canada, 1990.